

Borehole geophone repeatability experiment

Peter Gagliardi and Don C. Lawton

ABSTRACT

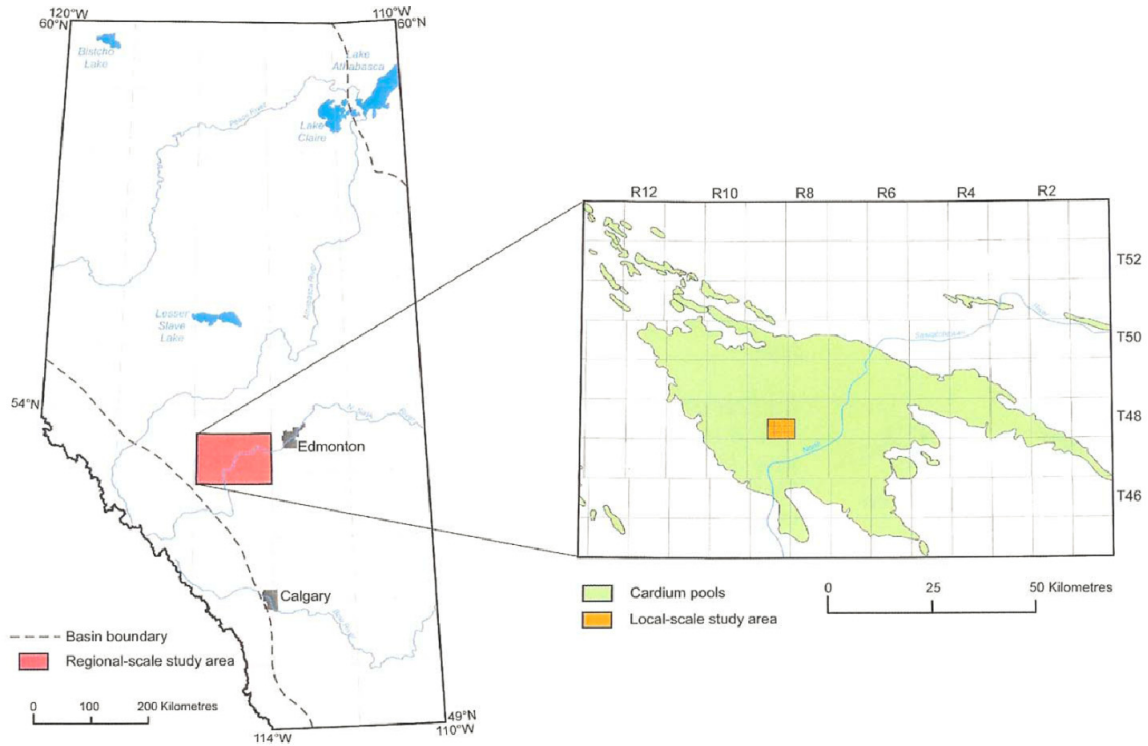
Time-lapse vertical seismic profile data was obtained near Violet Grove, Alberta, using an array of eight 3-component geophones at depths between 1497 m to 1640 m. Baseline data were recorded in 2005 and the monitor recorded in 2007. Analysis of rotation angles was undertaken for both surveys, resulting in differences of less than 2° for 54.2% in Line 2 and 85.9% in Line 3. Rotation angles were found to be more consistent at offsets greater than about 500 m. NRMS analysis gave averages of 61.4% and 45.3% for horizontal components, and 42.8% and 41.4% for the vertical component. Predictability analysis showed averages of 0.72 and 0.83 for horizontal components and 0.83 and 0.86 for the vertical component. In addition, traces were examined visually, and showed good qualitative repeatability. Since the receivers were cemented into place, the greatest effect on the repeatability was judged to be from small differences in the source locations between surveys, and differences in noise.

INTRODUCTION

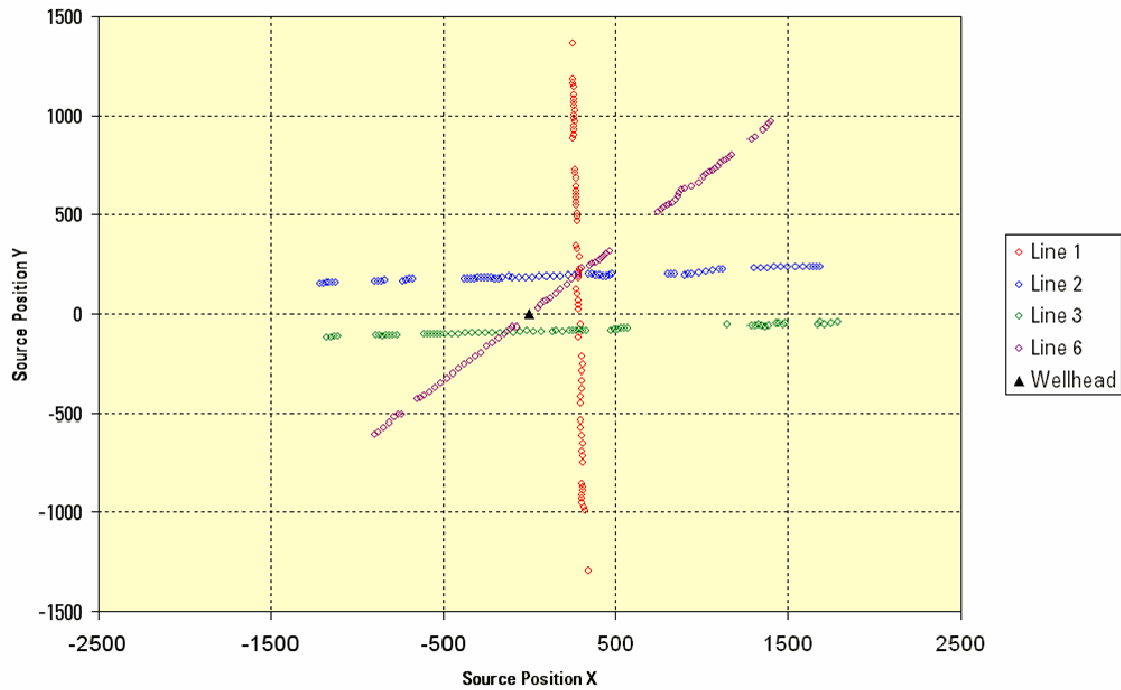
The Pembina CO₂ monitoring pilot has produced a wealth of interesting information regarding many geophysical and geological concepts, including CO₂ sequestration time-lapse geophysics. Over the course of this pilot, CO₂ was injected into the Cardium Formation in the Pembina oil field near Violet Grove, Alberta. A vertical seismic profile was recorded in an observation well 1650 m deep, using eight 3-component geophones placed roughly every 20 m starting at 1498 m depth (Hitchon, 2009). In this report, the Phase I (acquired in March 2005) and Phase III (acquired in March 2007) VSP data are studied for a repeatability analysis. This analysis includes the raw data of all three components, as well as examination of the calculated orientation angles for all geophones.

STUDY AREA

Out of several potential sites for a CO₂ monitoring pilot, the Pembina oilfield (Figure 1a) was judged to be the most promising. This oilfield is just over 100 km southwest of Edmonton and its major pool, in the Cardium, is the largest conventional oil pool that has been discovered in Western Canada (Hitchon, 2009). The seismic surveys consisted of three 2D lines: two parallel, east-west trending lines (Lines 2 and 3) and a north-south line (Line 1); the source used for all lines was dynamite. It should be noted that the data for Line 1 was corrupted and could not be used in this study. Furthermore, an additional line (Line 6) was acquired during Phase III. The geometry for this survey, including the location of the observation well 07-11-048-09W5, is shown in Figure 1b. The raw z-component data are shown in Figure 2 (Phase I) and Figure 3 (Phase III). In addition, some of the raw x and y-component data are shown side-by-side in Figure 4 (Phase I) and Figure 5 (Phase III).



(a)



(b)

FIG. 1. (a) Location of study area, in the Pembina oilfield. Figure from Dashtgard et al. (2006). (b) Acquisition geometry showing source locations and the well position; Line 2 and Line 3 are examined in this study.

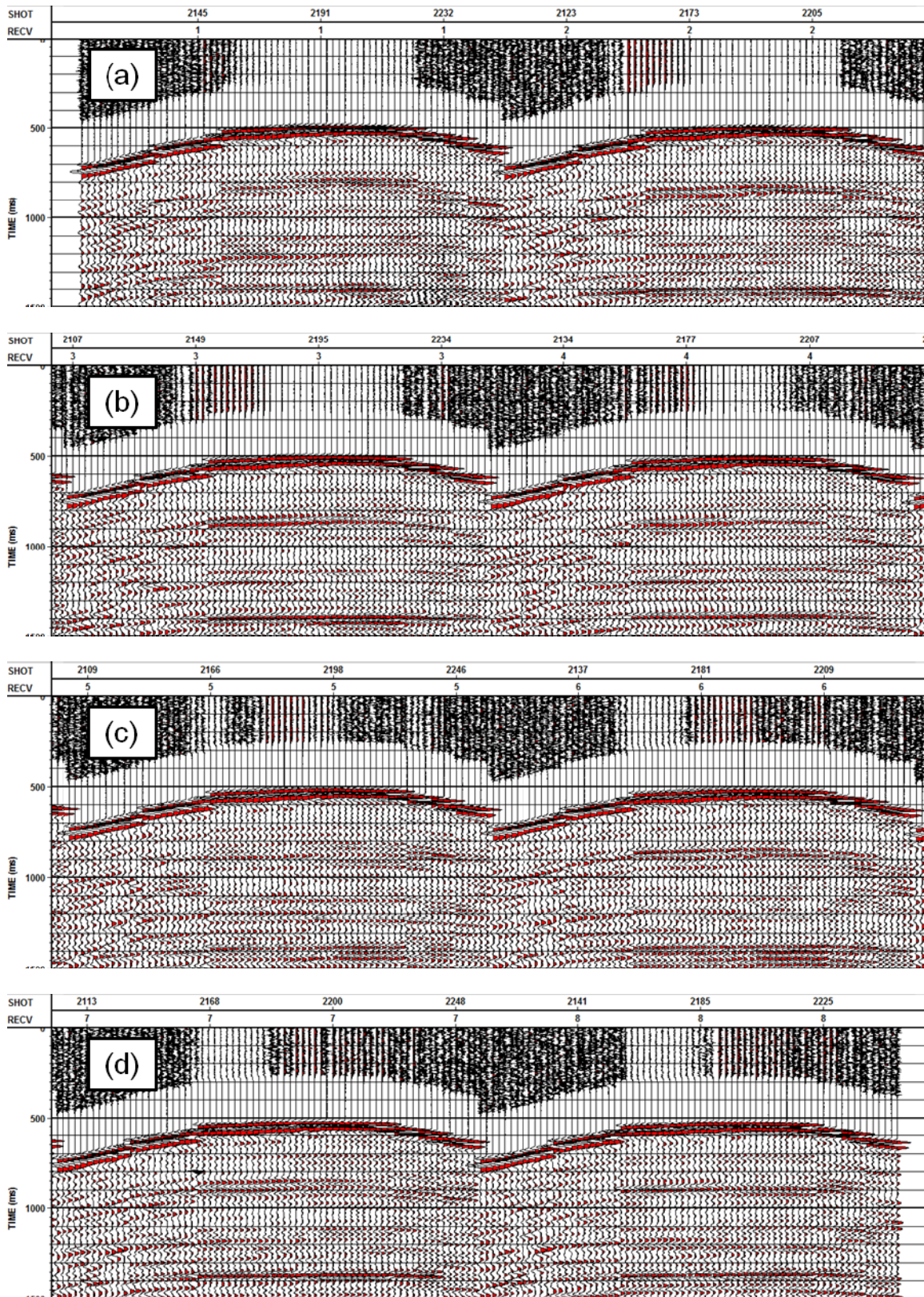


FIG. 2. Raw z-component geophone data with agc applied for Line 2 of Phase I for (a) receivers 1-2, (b) receivers 3-4, (c) receivers 5-6 and (d) receivers 7-8.

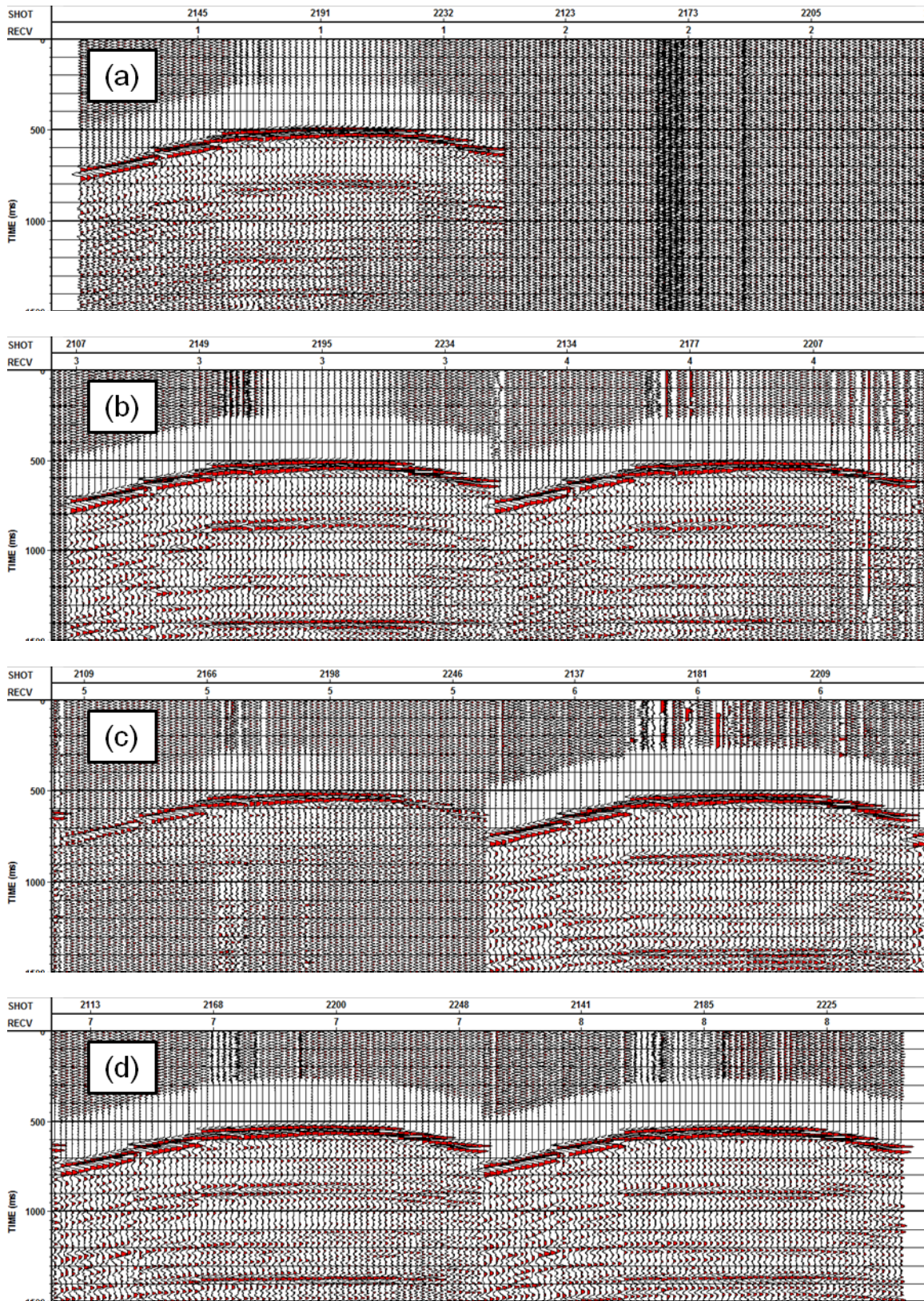


FIG. 3. Raw z-component geophone data with agc applied for Line 2 of Phase III for (a) receivers 1-2, (b) receivers 3-4, (c) receivers 5-6 and (d) receivers 7-8.

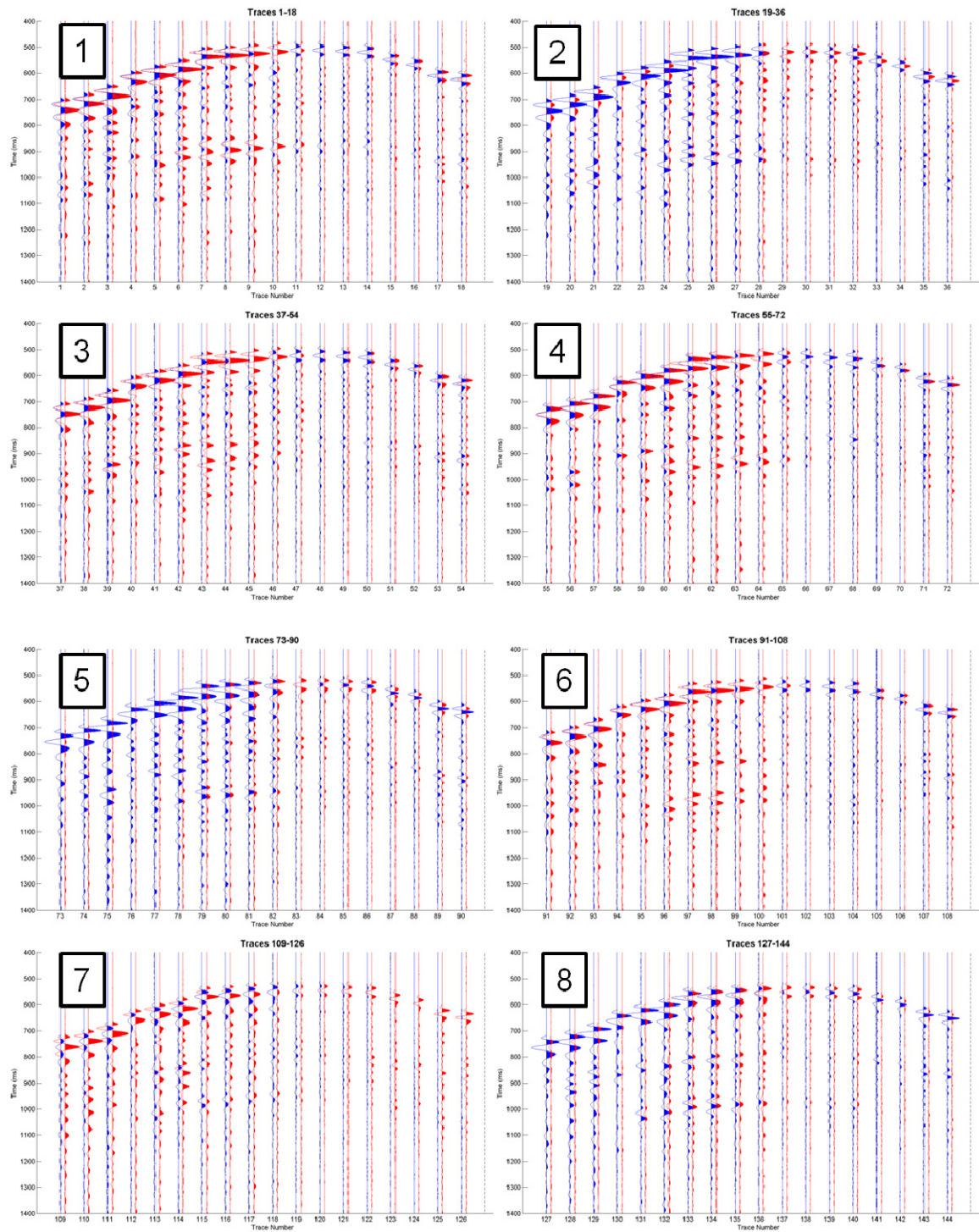


FIG. 4. Raw x and y-component for Line 2 of Phase I; receiver numbers are indicated on the top left corner of each trace. X-component is shown in blue and y-component is shown in red. Data was decimated to show every fourth shot.

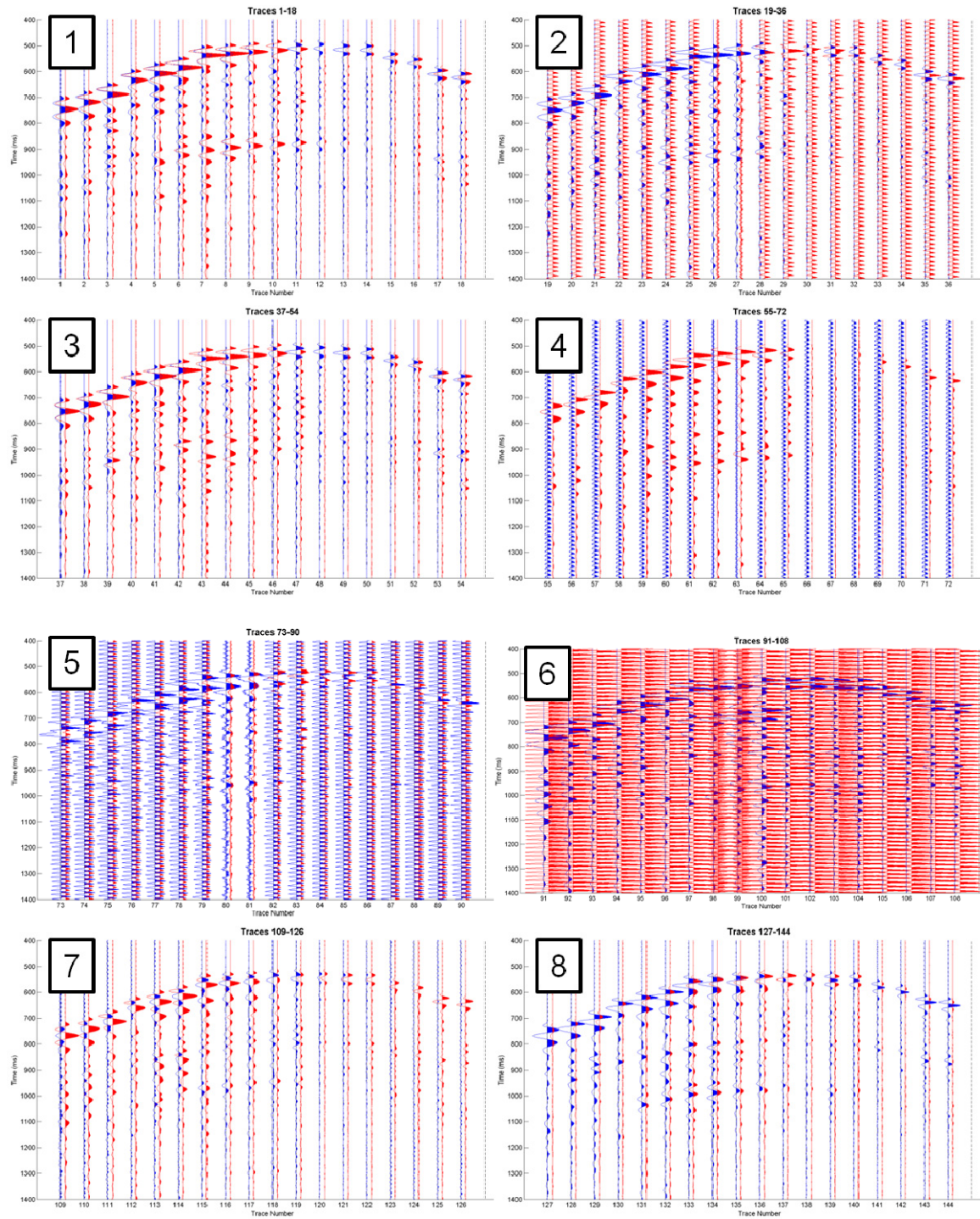


FIG. 5. Raw x and y-component data from 0.4 to 2 seconds for Line 2 of Phase III; receiver numbers are indicated on the top left corner of each trace. X-component is shown in blue and y-component is shown in red. Data was decimated to show every fourth shot. Note that receiver 6 needed to be rescaled due to the strong noise present in the y-component.

GEOPHONE ROTATION

Methods

Analysis was undertaken on the horizontal components of the data in order to determine the geophone orientation in the well. This was performed using the equation

$$\tan 2\theta = \frac{2X \otimes Y}{X \otimes X - Y \otimes Y}, \quad (1)$$

where \otimes is a zero lag cross-correlation operator, X is the windowed x-component data and Y is the windowed y-component data (DiSiena et al., 1984). In order to determine a window, first breaks needed to be picked; in this case, they were picked on the x-component data. Window lengths of 50 ms, 100 ms and 200 ms were tested, but for the purposes of this study only the results using the 100 ms window will be shown. Code was written based on equation (1) using the code from McArthur (2004) as a starting point.

Another common method used for finding geophone rotation is through the use of hodograms. Although analysis was performed using only the method described above, sample hodograms are shown in Figure 6. From these examples, it is clear that data from shots close to the well show more irregularity in their shape than the far offset shots. Examining the data quality of the x and y components, shown in Figure 5, illustrates the relationship between raw data quality and hodogram quality.

Consistency within surveys

Using the x and y-coordinates of each shotpoint, and using the x and y-coordinates of the well, source-receiver azimuths (θ_s) were calculated. In order to judge the consistency of each survey, the calculated geophone rotation angles were also converted into azimuths; Figure 7 shows histograms of these results. Except for receivers 4 and 6, the mean geophone azimuths were generally within about $\pm 2^\circ$. When only the farther offsets (those greater than 500 m) are examined (Figure 8) the dispersion decreases dramatically; this is an intuitive result, as farther offsets should contain more horizontal energy in general. Interestingly, while the standard deviations of the far offset angles are much lower, the mean values remain close to the mean values of the complete datasets (Table 1), given that both Line 2 and 3 (and thus the complete range of source azimuths) are considered.

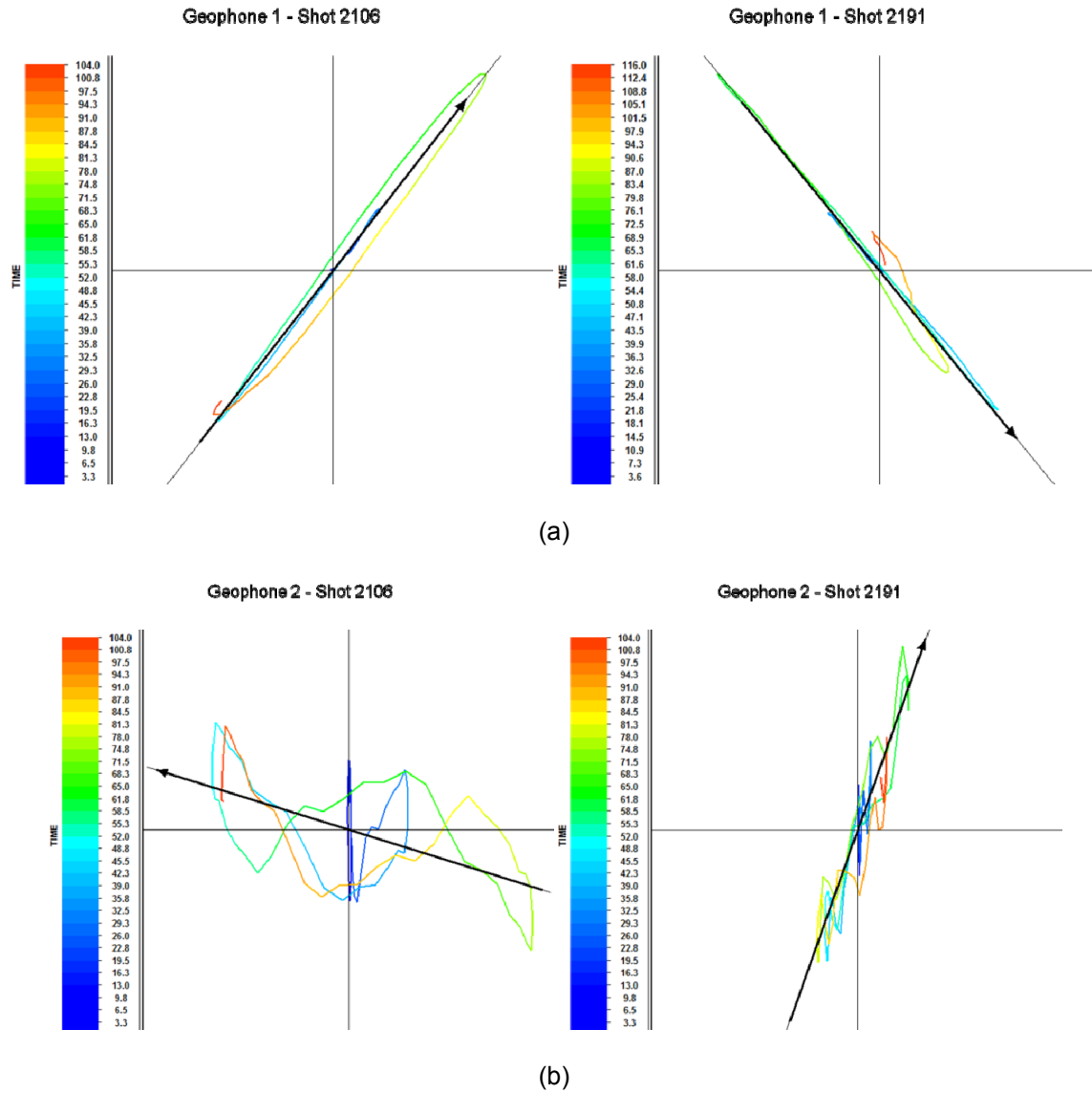


FIG. 6. Hodogram examples from Phase III, using a window of about 100 ms from the first breaks; shot 2106 (left) is a far offset and shot 2191 (right) is a near offset. Geophone 1 (a) had better data quality than geophone 2 (b), which is evident when examining the scatter of the hodograms.

Table 1. Means and standard deviations of geophone orientation angles for Phase I and Phase III, using all data and only far offsets.

Receiver	Phase I				Phase III			
	Mean (°)		Standard Deviation (°)		Mean (°)		Standard Deviation (°)	
Offsets	All	Far	All	Far	All	Far	All	Far
1	134.4	134.2	4.1	1.0	135.5	135.2	6.2	5.4
2	246.6	246.2	2.2	0.89	243.5	241.5	7.8	8.637
3	143.9	143.0	1.6	0.46	143.0	143.0	1.9	0.64
4	134.3	134.1	4.8	1.6	105.6	N/A	67.3	N/A
5	257.7	257.2	3.4	1.5	258.5	255.6	10.8	4.7
6	316.5	317.2	2.6	1.1	279.8	N/A	52.0	N/A
7	190.7	190.0	4.6	2.2	190.4	189.9	3.9	2.0
8	90.3	90.2	4.4	2.6	90.4	89.0	4.2	2.4
Average			3.4	1.4			19.3	4.0

The increased reliability of the far offset data can be seen clearly when the geophone azimuths are plotted against the source-receiver offset (Figures 9 and 10). Note that the source locations nearer to the well have much more scatter than those beyond about 500 m. Another interesting trend that can be seen is that geophone depth generally correlates to the offset required for consistent angle measurement. For example, geophones 1 and 2 appear to be approaching a stable angle faster than geophones 7 and 8. For Phase I, results were quite consistent within each line, and still fairly consistent between the two lines. For Phase III, however, some problems are evident. The noise on geophones 4 and 6 causes the angle calculations to become meaningless, exhibiting essentially only the trends of the well-shot azimuth; in addition, Line 2 seems to have a little bit of extra scatter compared to Line 3, especially for geophones 2 and 5.

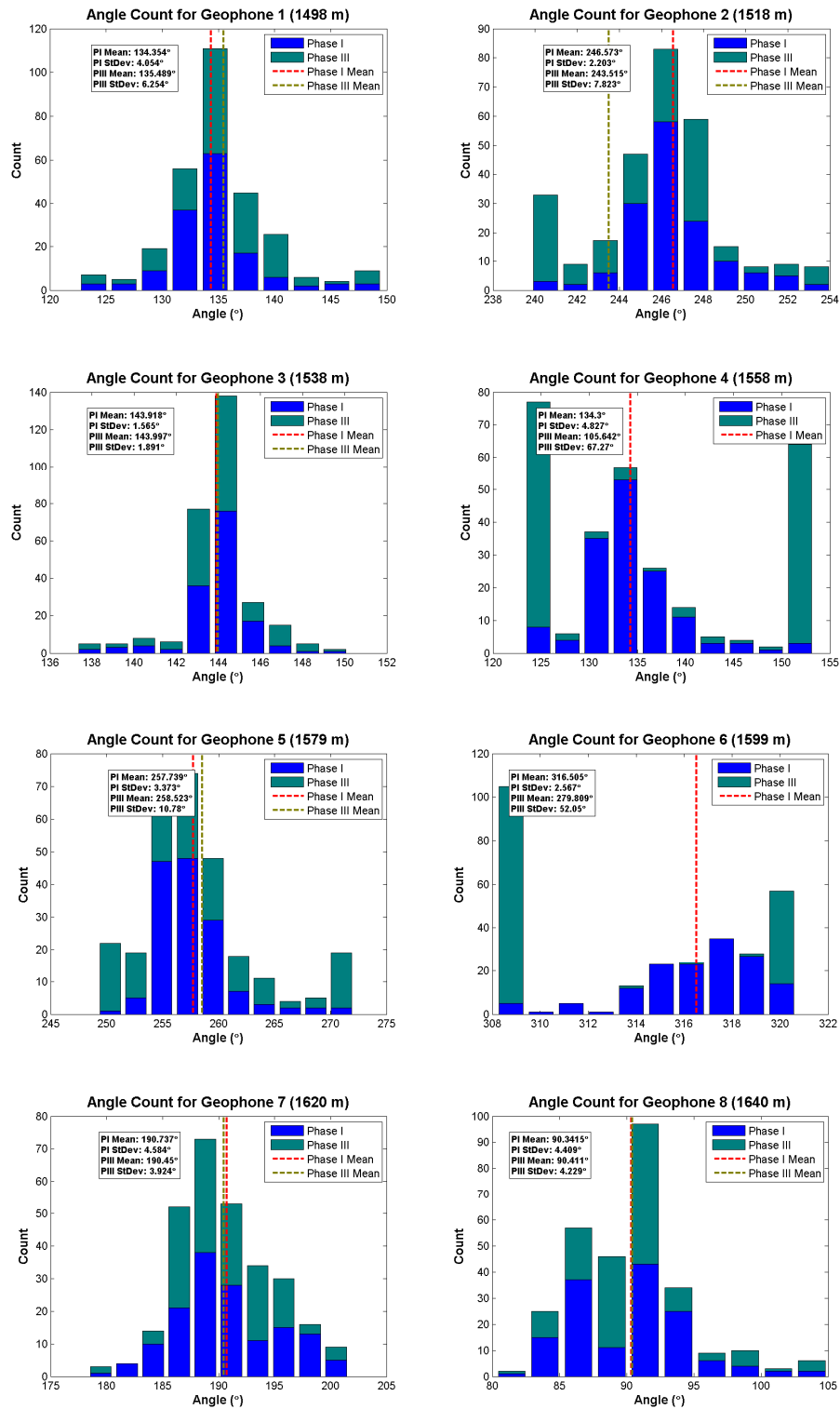


FIG. 7. Histograms of the calculated geophone azimuths; results include both lines. Phase I is shown in blue and Phase III is shown in green. Bin sizes were based on Phase I calculations. Dashed lines indicate means; Phase I is red and Phase III is dark yellow. Note that the Phase III means for receivers 4 and 6 are significantly different due to the high-amplitude noise on these geophones.

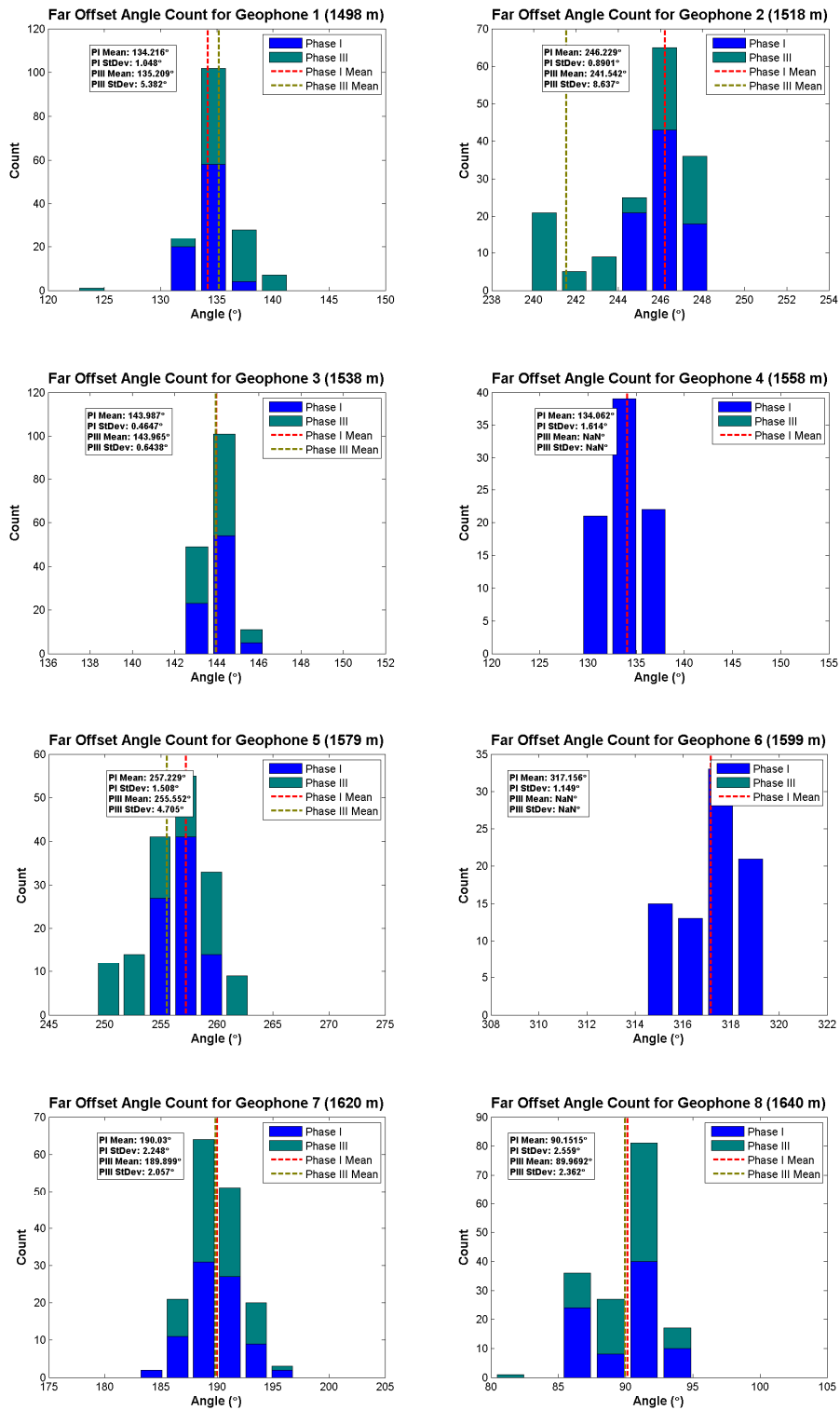


FIG. 8. Histograms of the calculated geophone azimuths, including only the far offsets (greater than 500 m); results include both lines. Phase I is shown in blue, Phase III is shown in green. Bin sizes were based on Phase I calculations using all offsets. Dashed lines indicate means; Phase I is red and Phase III is dark yellow. Note that receivers 4 and 6 don't show any Phase III data, due to the noise levels on these geophones.

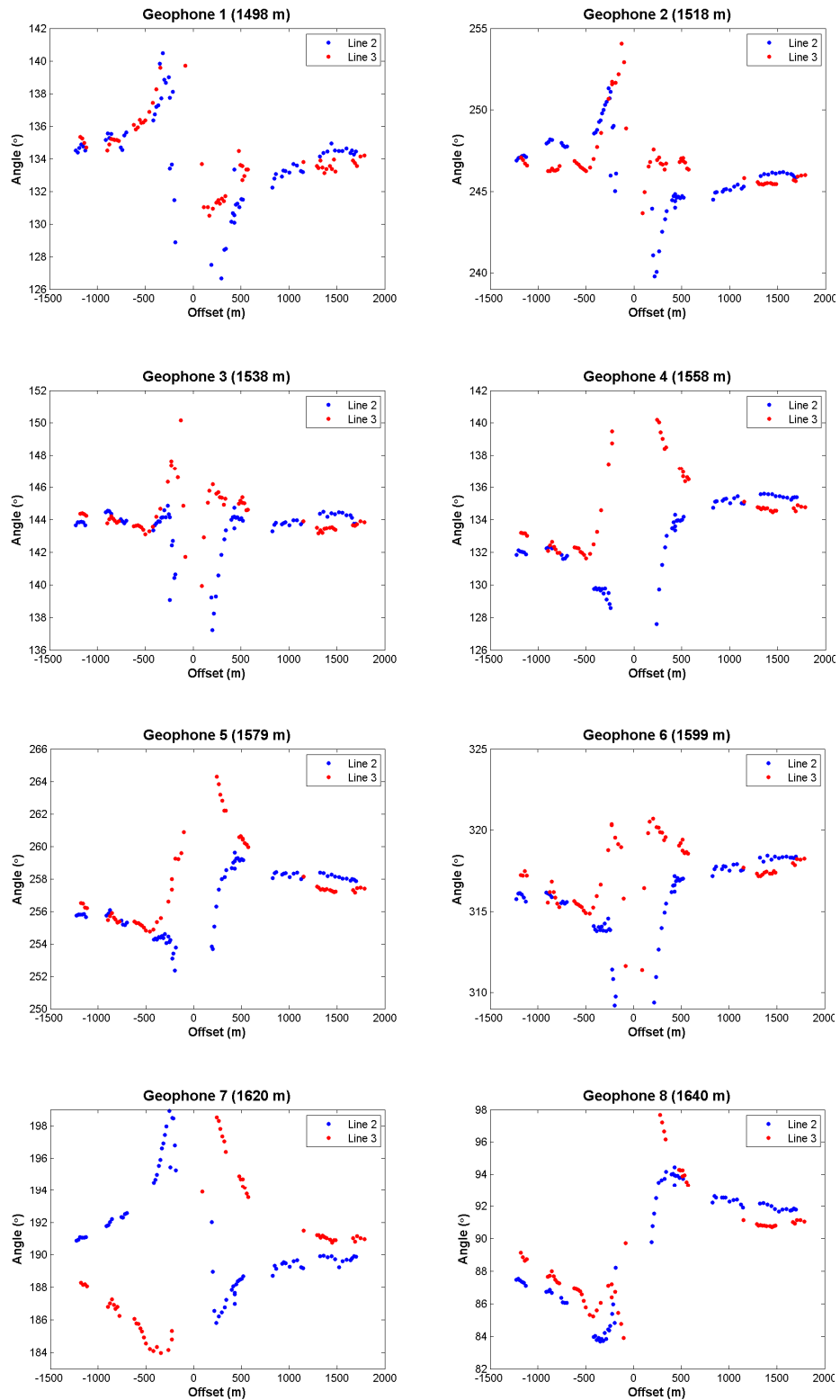


FIG. 9. Calculated geophone azimuths vs. source-receiver offset for Phase I. Line 2 is in blue and Line 3 is in red. All plots show a window of +/- 8° centered on the mean.

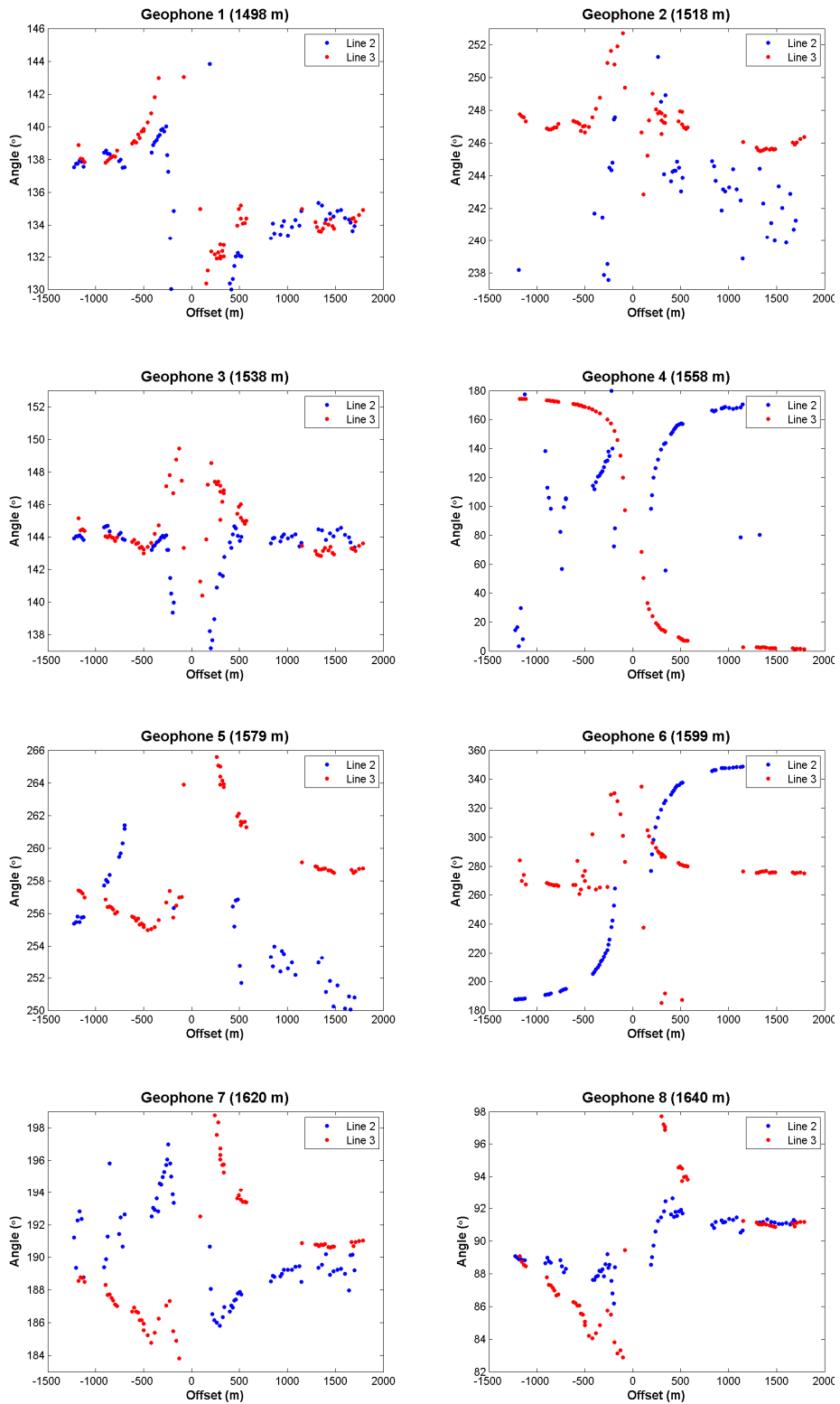


FIG. 10. Calculated geophone azimuths vs. source-receiver offset for Phase III. Line 2 is in blue and Line 3 is in red. All plots except 4 and 6 show a window of $\pm 8^\circ$ centered on the mean; this highlights the inconsistency of these two receivers.

Repeatability between surveys

Geophone azimuth comparisons between the Phase I and Phase III data were focused on individual shots. Figures 11 and 12 show orientation azimuth differences for each geophone; Table 2 catalogues the percentage of measurements that fall within various ranges.

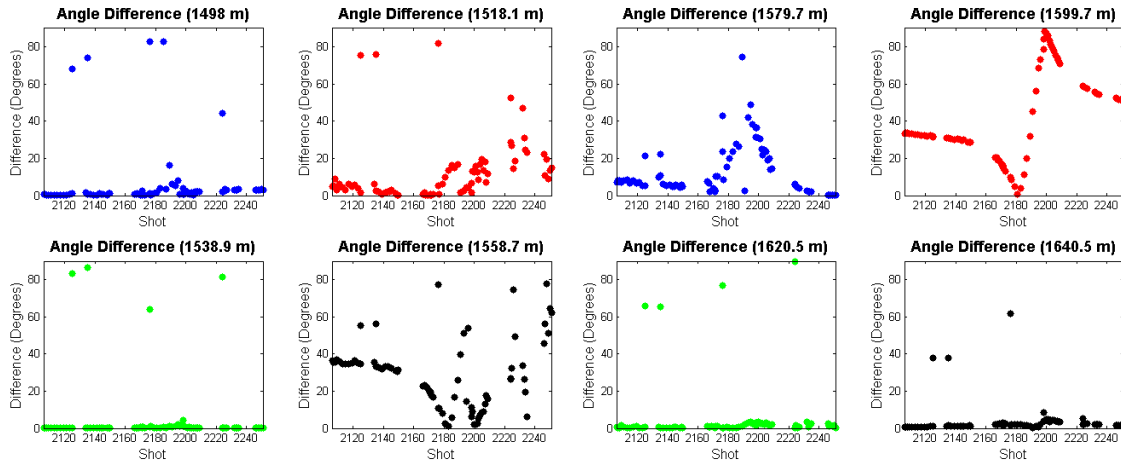


FIG. 11. Orientation azimuth differences for individual geophones (Line 2).

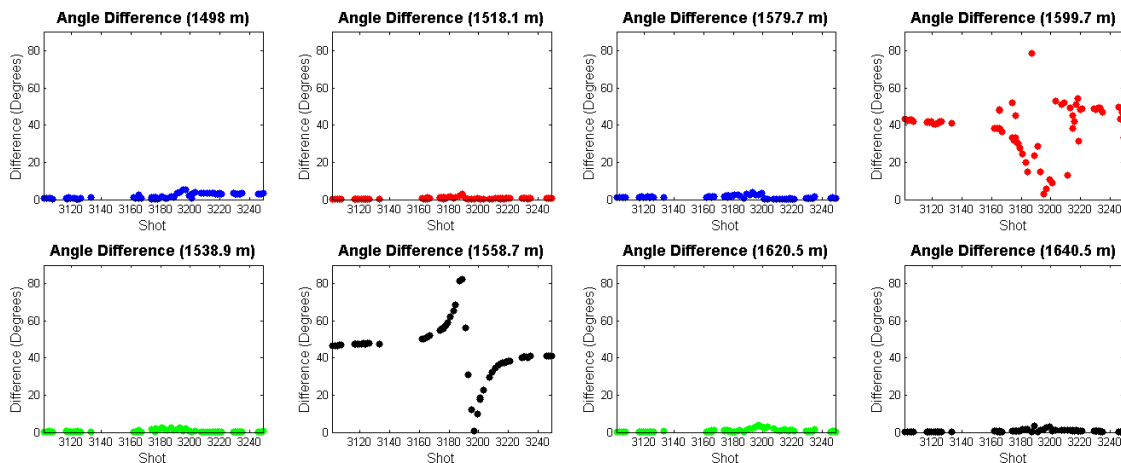


FIG. 12. Orientation azimuth differences for individual geophones (Line 3).

The results of the angle differencing are generally quite encouraging, especially those for Line 3. Closer analysis reveals that for Line 3, all but two of the geophones (4, at 1558.7 m, and 6, at 1599.7 m) are quite reliable and fall consistently within 5 degrees of error – this is only the case for half of the geophones in Line 2 (Table 2). If receivers 4 and 6 are ignored, the number of measurements within 2° improves to 54.2% for Line 2 and 85.9% for Line 3.

Table 2. Percentage of angle differences falling within 2, 5 and 10 degrees.

Receiver	Line 2			Line 3		
	Within 2°	Within 5°	Within 10°	Within 2°	Within 5°	Within 10°
1	61.8%	88.2%	92.1%	55.7%	97.1%	100.0%
2	26.3%	42.1%	60.5%	97.1%	100.0%	100.0%
3	92.1%	94.7%	94.7%	92.9%	100.0%	100.0%
4	2.6%	6.6%	18.4%	1.4%	1.4%	2.7%
5	10.5%	30.3%	61.8%	85.7%	100.0%	100.0%
6	1.3%	2.6%	7.7%	0.0%	1.4%	5.7%
7	75.0%	94.7%	94.7%	88.6%	100.0%	100.0%
8	59.2%	93.4%	96.0%	95.7%	100.0%	100.0%
Average	44.1%	56.6%	65.8%	64.6%	75.0%	76.1%

REPEATABILITY

Methods

There were two main repeatability metrics used in this study: nrms repeatability and predictability. Nrms repeatability is defined as (Kragh and Christie, 2002)

$$NRMS = \frac{200 \times RMS(a_t - b_t)}{RMS(a_t) + RMS(b_t)} \quad (2)$$

where a_t and b_t are the two input traces, the RMS operator is defined as

$$RMS(x_t) = \sqrt{\frac{\sum_{t_1}^{t_2} x_t^2}{N}} \quad (3)$$

t_1 and t_2 are the start and end times of the input window, and N is the number of samples in the window. For nrms, lower values generally correspond to better repeatability; the theoretical value that should be computed for complete noise is $\sqrt{2}$, which is roughly 1.41, or 141%. (Kragh and Christie, 2002)

Predictability is defined as (Kragh and Christie, 2002)

$$PRED = \frac{\sum \Phi_{ab}(\tau) \times \Phi_{ab}(\tau)}{\sum \Phi_{aa}(\tau) \times \Phi_{bb}(\tau)} \quad (4)$$

where Φ_{ab} is the crosscorrelation between traces a_t and b_t , using the time window t_1-t_2 . This metric will give higher values for more repeatable data (Kragh and Christie, 2002).

Only the zero lag values of the crosscorrelations will be considered in this report. The time window used for both metrics spanned the entire trace.

Horizontal component repeatability

In general, the repeatability on the x-component was slightly better than that of the y-component (Table 3). Similarly to the rotation data, Line 3 generally seems to have better repeatability than Line 2; in addition, it is quite evident which geophones recorded the poorest data during Phase III. It can be seen, upon individual examination of the receivers, that the average repeatability of Line 2 is being affected heavily by a few specific traces, whereas the average repeatability of Line 3 is much more consistent. This is quite noticeable if the data are plotted (Figures 13 and 14). Ignoring the x-component of receiver 4 and the y-component of receiver 6, the nrms average for both components drops to 61.4% for Line 2 and 45.3% for Line 3; the predictability rises to 0.72 for Line 2 and 0.83 for Line 3.

Table 3. Average nrms repeatability (NRMS) and predictability (PRED) values for the horizontal components of each geophone.

Receiver	Line 2				Line 3			
	Average NRMS		Average PRED		Average NRMS		Average PRED	
Component	x	y	x	y	x	y	x	y
1	26.8%	48.6%	0.96	0.78	42.4%	48.7%	0.86	0.81
2	29.2%	167.5%	0.94	0.04	40.1%	57.7%	0.87	0.73
3	23.7%	23.4%	0.97	0.96	41.7%	40.2%	0.86	0.87
4	153.5%	24.8%	0.00	0.96	178.6%	42.6%	0.00	0.86
5	155.8%	157.3%	0.10	0.09	50.1%	54.2%	0.79	0.76
6	24.0%	197.1%	0.97	0.00	41.0%	164.6%	0.86	0.00
7	83.0%	29.3%	0.55	0.94	46.5%	42.2%	0.83	0.85
8	31.6%	34.5%	0.93	0.91	44.5%	40.7%	0.84	0.87
Average	65.9%	85.3%	0.68	0.59	60.7%	61.4%	0.74	0.72

If this repeatability analysis is compared directly to the orientation angle analysis, it might be logical to assume that the same trends would be evident; interestingly, however, this is not quite the case. Two good examples of this are receivers 3 and 8. In both cases, the repeatability metrics indicate that Line 2 has better repeatability over Line 3, while the angle differencing indicates the opposite. Another contrast is between receivers 1 and 5 in Line 3: the repeatability metrics suggest that receiver 1 is more repeatable, but angle differencing clearly contradicts this.

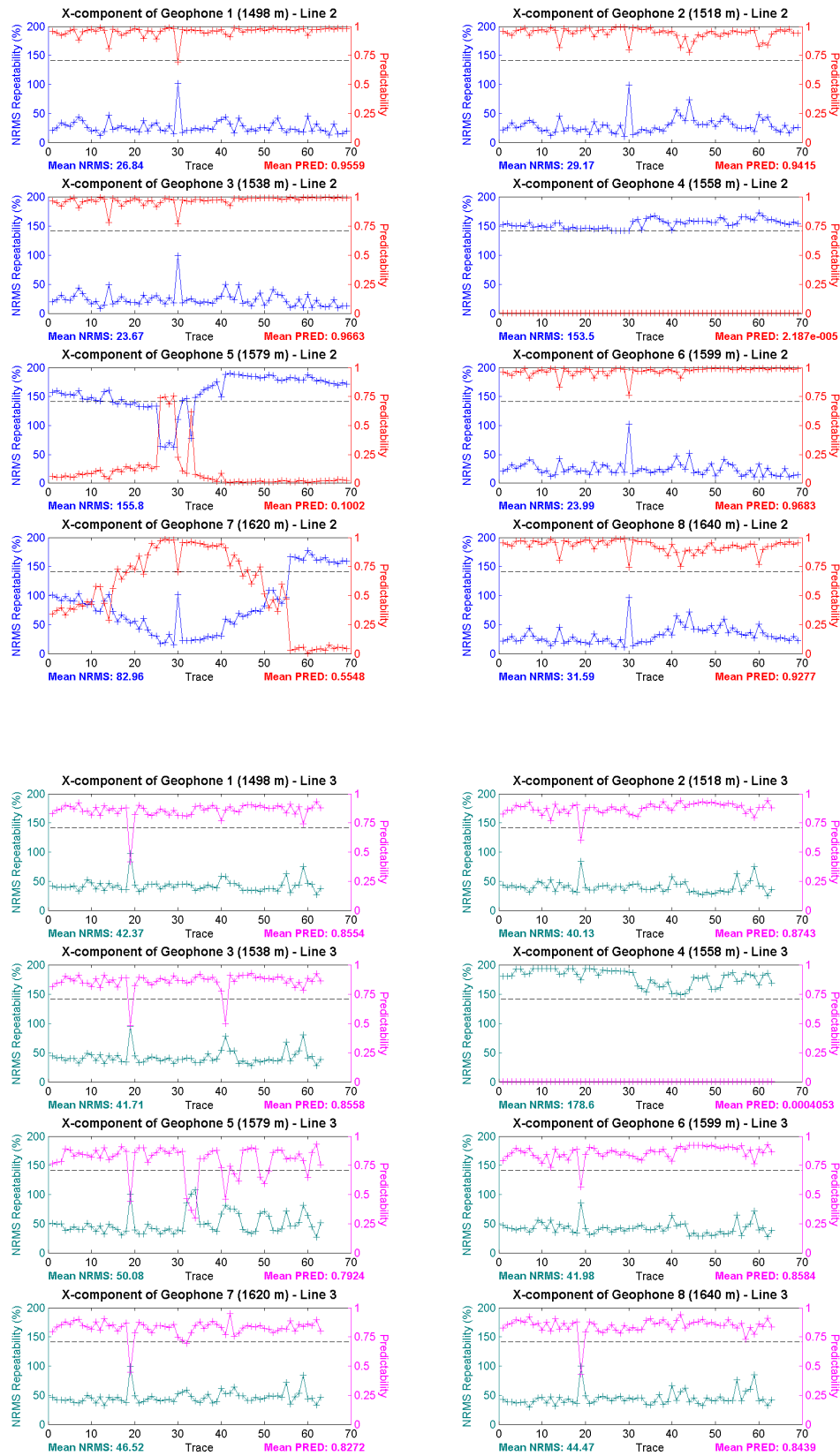


FIG. 13. Nrms repeatability and predictability of the x-component for Line 2 (top) and Line 3 (bottom). The horizontal dashed line indicates the nrms repeatability for random noise.

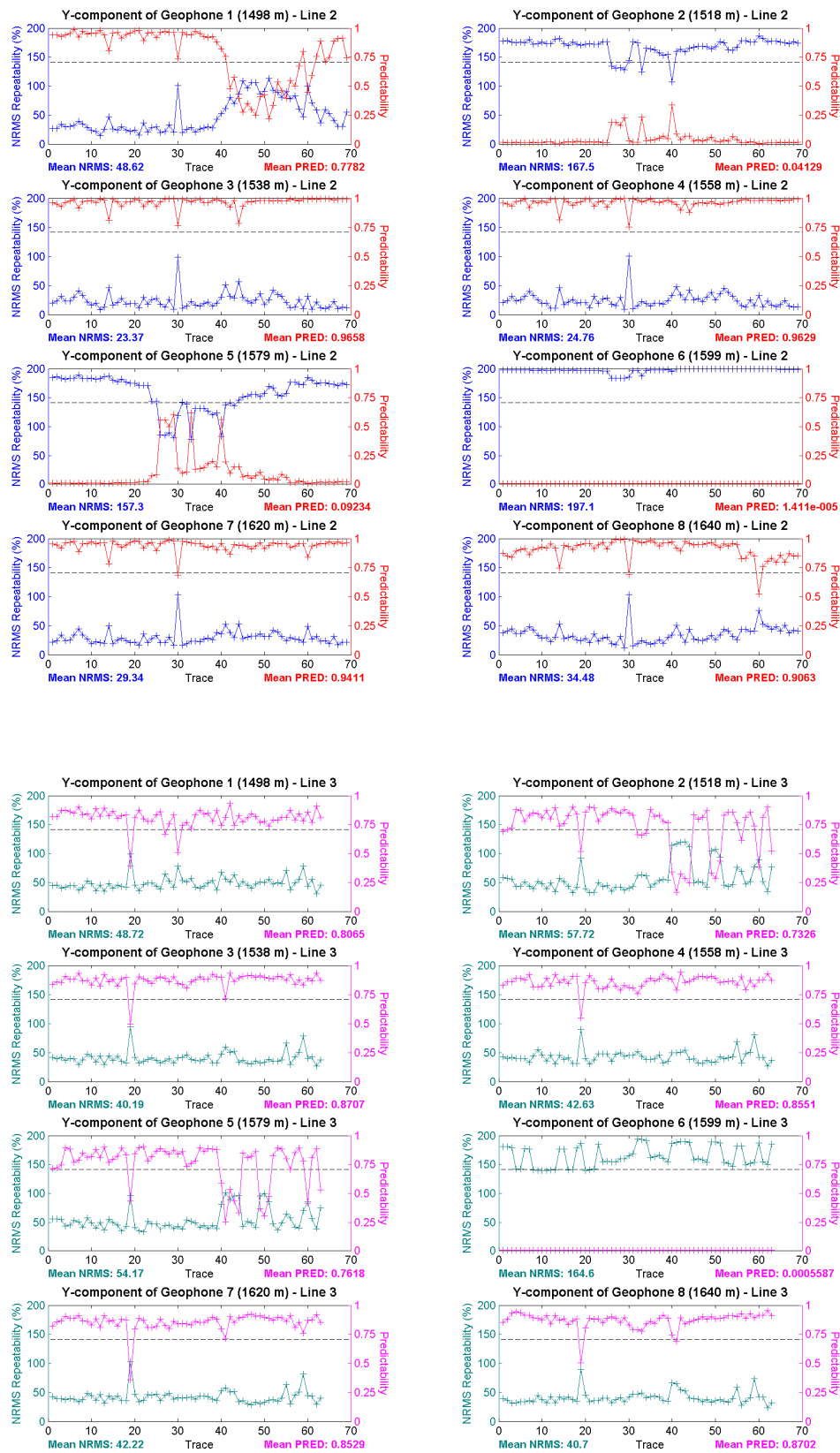


FIG. 14. Nrms repeatability and predictability of the y-component for Line 2 (top) and Line 3 (bottom). The horizontal dashed line indicates the nrms repeatability for random noise.

Vertical component repeatability

Repeatability of the vertical component was overall better than either of the horizontal components. Values in Table 4 show that Line 2 shows better repeatability for all but two of the receivers (1 and 5). This is an improvement over both the x and the y-component data, which each had three bad receivers. Line 3 repeatability is much more consistent between all three components, providing differences within about 7% in nrms values and within 0.05 in predictability values. Once again, the better consistency of Line 3 is more evident when examining plots of the data (Figure 15). Ignoring receiver 2 changes average nrms to 42.8% for Line 2 and 41.4% for Line 3, and improves average predictability to 0.83 for Line 2 and 0.86 for Line 3.

Table 4. Average nrms repeatability (NRMS) and predictability (PRED) values for the vertical component of each geophone.

Receiver	Line 2		Line 3	
	Average NRMS	Average PRED	Average NRMS	Average PRED
1	49.5%	0.79	44.2%	0.86
2	151.9%	0.00	192.0%	0.00
3	24.5%	0.96	41.2%	0.87
4	39.9%	0.86	44.3%	0.84
5	108.4%	0.34	42.4%	0.86
6	25.4%	0.96	39.6%	0.88
7	26.0%	0.95	40.8%	0.87
8	24.5%	0.96	37.1%	0.90
Average	56.4%	0.73	60.3%	0.76

Trace overlaps

While nrms repeatability and predictability provide a useful and quantitative measure of repeatability, seismic interpretation is visual in nature and as such a more visual, qualitative approach is also useful. Code was developed in MATLAB to compare the two phases of data by plotting the traces on top of each other; this allows for a direct visual comparison between corresponding traces. Figure 16 shows recordings of all three components at shotpoint 2191, taken in a time window from 450 – 900 ms. There are many cases where the traces line up nearly perfectly, however subtle differences are noticeable. For example, the first breaks in the z-component show generally higher amplitudes in the Phase I data then they do in the Phase III data.

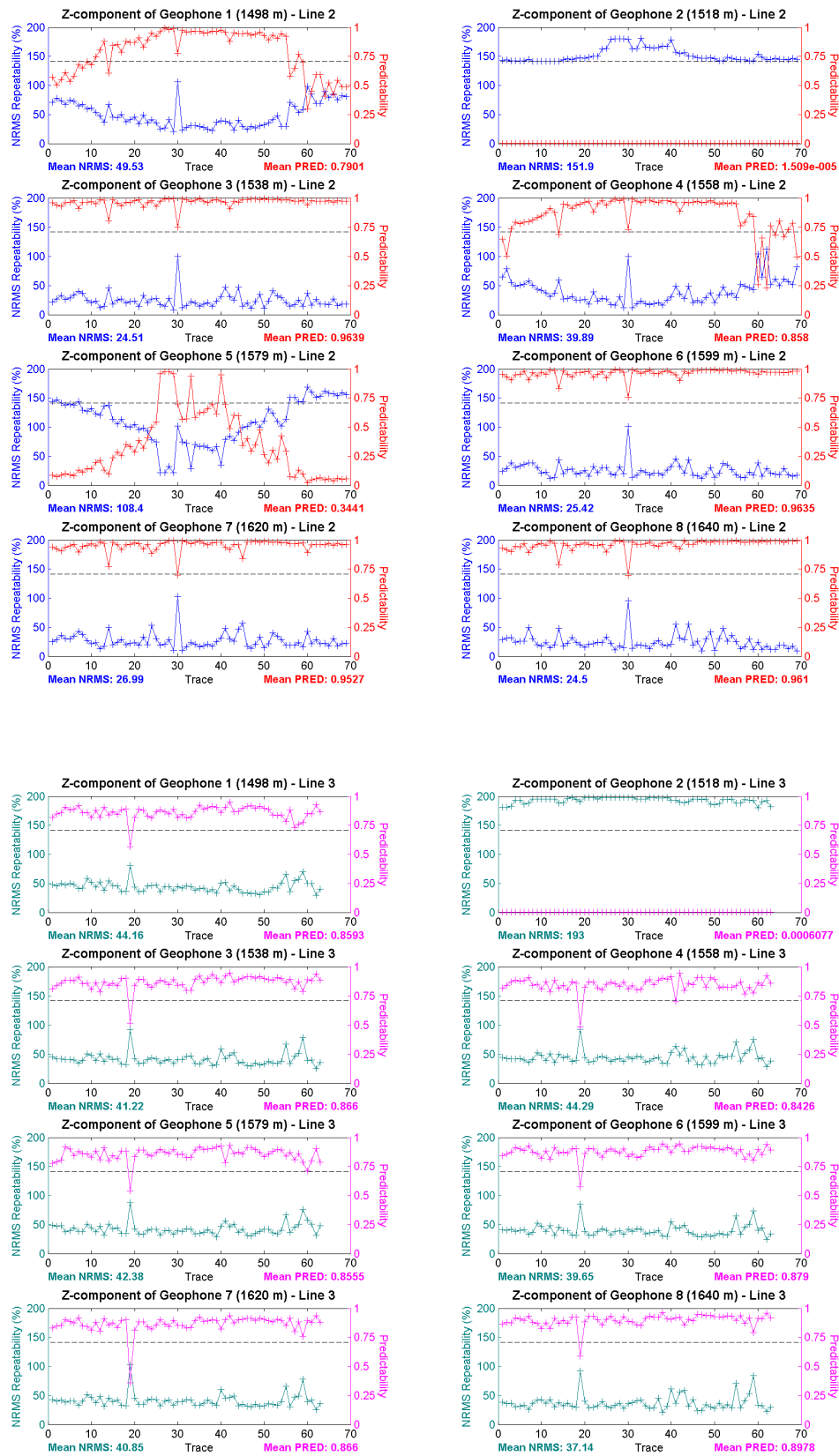


FIG. 15. Nrms repeatability and predictability of the z-component for Line 2 (top) and Line 3 (bottom). The horizontal dashed line indicates the nrms repeatability for random noise.

Shot 2191

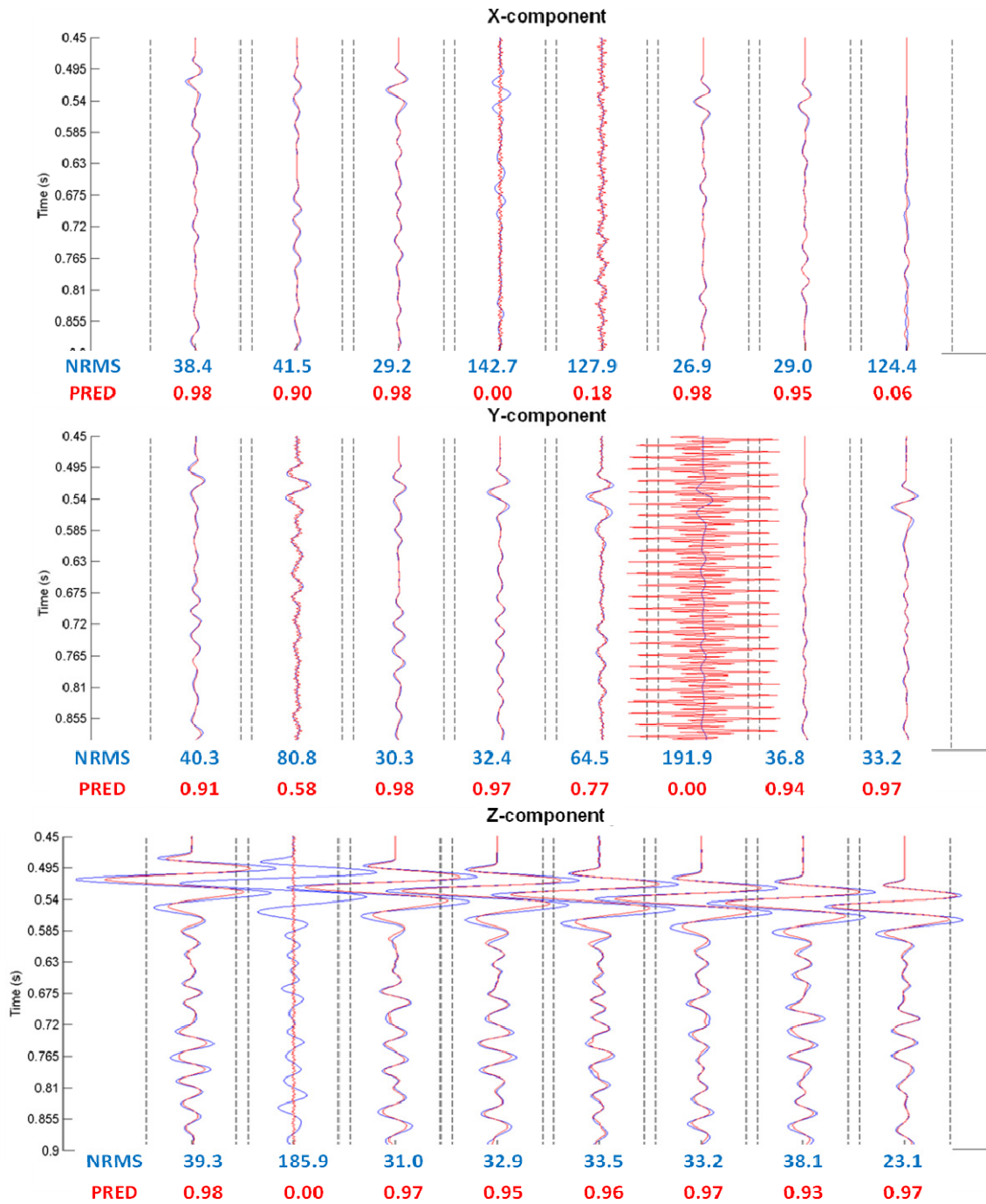


FIG. 16. Trace overlaps of all three components for shot 2191, with nrms and predictability below each trace. Phase I is in blue, Phase III is in red. Black dashed lines indicate an amplitude envelope of ± 1 .

DISCUSSION

Overall, repeatability of the raw VSP data showed that there were some issues related to noise. These problems were partially due to hardware problems with the receivers in Phase III acquisition; these issues resulted in the complete loss of data for three out of twenty-four possible traces. Furthermore, strong noise was introduced to two more traces that were quiet in Phase I. However, even if the effects of these five traces are ignored, it still results in somewhat low repeatability values for this survey. Studies, such as Cantillo et al. (2010), show that the factor which most strongly affects repeatability metrics is the difference in source positioning; since the geophones were cemented into the well (and therefore receiver positions are constant) it can be inferred that the negative effects on the repeatability metrics are almost completely due to small changes in source positioning, source coupling, and changes in the subsurface. CO₂ movement in the subsurface is expected to affect repeatability, although the extent of this is not clear at this time.

Due to the fact that only five of the geophones had useable data in all three components, processing has only been done on the vertical data (Daniels, 2008); however, despite the poorer data quality of the horizontal components, it would be interesting to see what a full processing flow can obtain in terms of converted wave data. In addition, once the data are processed, stacked and migrated, the repeatability is expected to show improvement.

The results from the geophone orientation calculations are more encouraging. The agreement here is quite good between surveys, especially in Line 3. While these results agree with the other repeatability metrics in the better consistency of Line 3, they do occasionally have opposite trends – the reasons for this are not clear at the moment, but it does present a potentially interesting topic for future investigations. The relationship between azimuth scatter, offset and receiver depth is interesting, and could have implications regarding ideal acquisition geometry in the case of 3-component VSP surveys.

CONCLUSIONS

- Repeatability of the Violet Grove VSP dataset was found to be of medium quality when considering all the raw data.
- Receivers 2, 4 and 6 each had severe problems with one of their components during Phase III, meaning that only five of eight geophones yielded good data on all components in both surveys.
- Within surveys, angle calculations using offsets greater than 500 m were shown to be much more consistent than those using near offsets. However, when the full range of source locations were considered, the mean values calculated for geophone azimuths did not significantly change when the near offsets were excluded, suggesting that statistical analysis of this parameter is fairly reliable across all offsets.

- Repeatability in rotation, ignoring receivers 4 and 6, showed that 54.2% of Line 2 shots and 85.9% of Line 3 shots were within 2° between surveys, and that the mean azimuth values generally had less than a 1° difference.
- Nrms repeatability of working horizontal components averaged to 61.4% for Line 2 and 45.3% for Line 3, while predictability was 0.72 and 0.83 respectively.
- For functioning vertical component data, the nrms for Line 2 and 3 averaged to 42.8% and 41.4% with predictability of 0.83 and 0.86, giving better and more consistent results than the horizontal component data.
- Visual examination of traces showed subtle differences in all three components, but overall showed close correlation between Phase I and Phase III data.
- The strongest negative effect on the repeatability was interpreted to be differences in source locations and differences in noise, since receiver positions were held constant between surveys.

FUTURE WORK

Only the raw data were examined in this study. For future studies, the data will be taken through a full processing flow, ideally making use of all three components, and repeatability re-examined. In addition, the relationship between receiver depth and angle consistency will be examined, and differences in the data will be used to try and image movement of CO₂ in the subsurface.

ACKNOWLEDGEMENTS

We would like to thank Penn West and Schlumberger for the data used in this study, GEDCO for the use of their Vista software, and all CREWES sponsors for continued support of our research.

REFERENCES

- Cantillo, J., Boelle, J., Lafram, P. A. and Lecerf, D., 2010, Ocean Bottom Nodes (OBN) repeatability and 4D: SEG Expanded Abstracts, **29**, 61-65.
- Daniels, S., 2008, Time Lapse VSP Processing Report: Schlumberger,
- Dashtgard, S. E., Buschkuehle, M. B. E., Berhane, M. and Fairgrieve, B., 2006, Local-Scale Baseline Geological Report for the Pembina-Cardium CO₂-Enhanced Oil Recovery Site: Alberta Geological Survey,
- DiSiena, J. P., Gaiser, J. E. and Corrigan, D., 1981, Three-component vertical seismic profiles; orientation of horizontal components for shear wave analysis, in Toksoz, M. N. and Stewart, R. R., eds., Vertical seismic profiling, Part B Advanced concepts, , 189-204.
- Hitchon, B., 2009, Pembina Cardium CO₂ Monitoring Pilot: A CO₂-EOR Project, Alberta, Canada: Final Report: Geoscience Publishing, Limited.
- Kragh, E. and Christie, P., 2002, Seismic repeatability, normalized rms, and predictability: The Leading Edge, **21**, 640-647.
- McArthur, M. A., 2004, Velocity Structure and Seismic Imaging of a Shallow Coal Zone, Red Deer, Alberta: B.Sc. thesis, University of Calgary.